Long-term changes in sea-level components in Latin America and the Caribbean

I.J. Losada*[1], B.G. Reguero[1], F.J. Méndez[1], S. Castanedo[1], A.J. Abascal[1], R. Mínguez[1]

[1] Environmental Hydraulics Institute "IH Cantabria", Universidad de Cantabria, Spain
* Corresponding author

Manuscript submitted to: Global and Planetary Change
Date of submission: 19/09/2012

Corresponding author address
Environmental Hydraulics Institute, IH Cantabria
Universidad de Cantabria
C/ Isabel Torres nº 15
Parque Científico and Tecnológico de Cantabria
39011, Santander, SPAIN

Phone: +34-942-201414
e-mail: losadai@unican.es

Abstract

Mean Sea-Level is not the unique factor that should be considered in rising sea levels since storm surges and changes in extreme events may also have a bearing in the coastal problems. In this study, we use astronomical tide, mean sea-level and storm surges to explain changes detected in the various components conforming the sea-level in the region of Latin America and the Caribbean. Methods based on a non-stationary extreme value analysis were applied to storm surge and total sea elevations monthly maxima for the last six decades, while long-term trends in Mean Sea-level were computed with a trend-EOF technique. Besides, the relative importance of each factor contributing to the total sea-level is explored through its statistical distribution. Results show that a clear correspondence can be found through a simple regression model between Mean Sea-Level and the Niño3 climate index, which in turn explains more than 65% of the variance. The analysis further demonstrates that concerns should be focused on different components of sea-level in the various areas included in our study. For example, the changes in the storm surge levels are a key stressor in the Río de la Plata area, while the increase in the extreme total sea-levels in the tropical region and the influence of inter-annual variability on its western coast are the prominent factors.

Keywords

Inter-annual variability; Latin America and the Caribbean; Sea-level components; Sea-level rise; Storm surge; Non-stationary extremes

Highlights

- Description of the various sea-level components through the reconstruction of Astronomical Tide, Storm Surge and Mean Sea-Level time series
- The relative weight of each sea-level component is analyzed for the region of Latin America and the Caribbean
- Significant variations in long-term trends in mean sea-level and extremes in storm surge and total sea-level were found.
- Strong correlations with some climatic indices were found for mean sea-level and storm surge
- The Niño3 index shows a strong linear relationship with mean sea-level in the tropical Pacific coast

1. Introduction

Coastal zones are among the most vulnerable areas to climate change, facing various impacts arising from this cause. Among these, rising sea-levels sometimes combined with subsidence, have been shown to lead to flooding, coastline erosion, impacts on ecosystems or salination of aquifers (Ericson et al., 2006; Syvitski et al., 2009; Nicholls and Cazenave, 2010). Such problems demand measures for adaptation, and integrated coastal management (Nicholls, 2011). However, the first step is to thoroughly understand the past changes in the specific areas of study, at an adequate spatial scale, where the impacts are to be inferred. Additionally, understanding which are the major factors contributing to total sea-level is required to lead efforts towards further analysis, prevention and adaptation solutions to flooding and erosion. To that end, this work offers a comprehensive understanding of the different sea-level components in Latin America and the Caribbean region (LAC).

Time series of Total Sea-Level (TSL) result from the combination of several components which vary both temporally and spatially: (1) mean sea-level (MSL); (2) Astronomical tide (AT), which oscillates on the MSL in a scale of hours and (3) surges produced by wind and pressure, commonly known as Storm Surge (SS). Breaking waves also cause sea-level changes in the surf-zone, called swell set-up, which depend on local coastal characteristics. This factor is however not analyzed here, our main focus centered on sea-level variations at deeper waters; so local surf zone features, are not taken into account.

In general, Sea-Level Rise (SLR) is the name given to changes detected over various years in the MSL. Moreover, land subsidence relative to the sea causes additional displacement to be added to the SLR, the combination of which is known as Relative Sea-Level Rise (RSLR). Aggregation of the different components forms hourly

TSL time series whose analysis may determine the flooding statistic on different time scales. This makes it necessary to define all the components influencing sea-level rise, as well as their relative overall weight in order to make a correct statistical analysis of possible impacts. For example, Nicholls (2004) showed that the effects of a given MSL rise in estuaries will have different effects in macrotidal and microtidal environments.

Rising sea-levels have been extensively studied in the recent years (e.g., IPCC, 2007; Cazenave et al., 2008; Church et al., 2010; Rignot et al., 2011; or de Santis et al., 2012). However, as suggested in Walsh et al. (2012), changes in sea-level extremes are the upshot of different combinations of MSL, local trends, the incidence of storms (including tropical storms and cyclones) and the marine climate. The combination of these factors and their relative importance define coastal flooding threats worldwide. Sea-level extremes occur not only under high SS values combined with AT. Sometimes high rises due to AT and moderate SS values can pose a flooding risk on particular coasts. Even where SS is the predominant factor, there may be non-linear combinations of SS and AT which must be taken into account (Horsburgh and Wilson, 2007). This is why flooding studies must take into account the accumulated effect of the different components of sea-level. The combination of rising sea-levels and storm surges has already been dealt with at a global scale in several studies (Dasgupta et al., 2009), and specifically for particular areas of the LAC region (Fiore et al., 2009).

As far as we know, in our study region there is no information on changes in MSL, AT and SS, or TSL with a sufficient degree of resolution and a discussion on the relative importance of each factor is lacking. Therefore, this paper aims to: (1) explain the changes observed in the various sea-level components in LAC, (2) examine changes in TSL extremes and (3) discuss the relative importance of each of the contributing factors. In order to achieve these goals, we used instrumental MSL data to infer past changes, employing two different long-term trend assessment statistical techniques. The relative importance of SLR with respect to the MSL seasonality is also studied. The SS was modeled numerically (without including hurricanes, i.e.: excluding tropical storm extremes tails) to study the changes in this component. Finally, considerations on the influence of climatic patterns on each variable on a continental scale are also addressed.

To structure the work, the section following this introduction describes the sources of information of the data and explains the statistical methods used for the extremes analysis and the determination of the long-term trends. Section 3 deals specifically with the study of sea-level components, their changes and their relative importance in different parts of the continent. A brief discussion follows in section 4 on the climatic patterns with the highest influence on each component. Finally, section 5 highlights the most important conclusions.

2. Regional Setting

The area of study is the region of the Atlantic and Pacific Ocean basins that wash the coasts of Latin America and the Caribbean (LAC). With a total coastline length of about 72,182 km this region is highly variable in terms of coastal dynamics and geomorphological features. From the varying conditions in the Atlantic and Pacific, the Caribbean Sea is a third area with particular characteristics. Covering from high latitudes in the Southern Ocean to equatorial areas, generally, little knowledge is available on the different sea-level components and its temporal past changes for the whole region.

3. Data and Methods

3.1. Data

The area of study includes the coast of Latin America and the Caribbean (LAC), a total of approximately 72,182 km of coast (see Figure 1). Several sources of instrumental and numerical data were used to evaluate the sea-level components in the LAC region. Table 1 summarizes the variables considered and the original source, as well as their time span and spatial resolution.

Data source	**Variables**	**Time span**	**Time resolution**	**Spatial Resolution**
CSIRO	Mean Sea-level(MSL)	1950-2009	monthly	Global, 1º
	Mean Sea-level anomaly			
TPXO dataset	Astronomical Tide (AT)	harmonic constants	hourly	Global, 0.25º
Tidal Gauges (UHSLC)	Mean Sea-level(MSL)	Variable	hourly	Global, variable
	Storm Surge (SS)			
Numerical Reanalysis (GOS)	Storm Surge (SS)	1948-2008	hourly	LAC, 0. 25º

Table 1. Sources of information of the variables considered, their time span and spatial resolution.

MSL data were obtained from the Commonwealth Scientific and Industrial Research Organization (CSIRO) and can be downloaded at: http://www.cmar.csiro.au/sealevel/sl_data_cmar.html. These data provide monthly MSL series on a 1º x 1º (longitude x latitude) grid of spatial resolution between 65°S and 65°N, from 1950 to present, although for this study we used 2008 as the last year of analysis. Between 1950 and 2001 the sea-level information was reconstructed from tidal gauges (Church et al., 2004), and the 1993-2008 data come from TOPEX/Poseidon, Jason-1 and Jason-2/OSTM mission altimeters. Data were deseasonalized and include an inverse barometer correction, following the correction for glacial isostatic adjustment.

Tidal gauge data were obtained from Hawaii University's Sea-level Center (UHSLC) and used to compare the results of the AT and the SS time series. These data are available at http://ilikai.soest.hawaii.edu/uhslc/rqds.html. Locations are presented in Figure 1 along with the identification codes of the tidal gauges shown in this paper for validation. The data series provide hourly time resolution, and register longitude variations for each station.

AT data were generated on the LAC coasts using the harmonic constants derived from the TPXO global tides model (version 7) developed by Oregon State University (Egbert et al., 1994; Egbert and Erofeeva, 2002). The TPXO model assimilates data from the TOPEX/Poseidon missions and tidal gauges (Ardalan and Hashemi-Farahani, 2007). The database includes eight primary harmonic constants (M2, S2, N2, K2, K1, O1, P1, Q1) and two long period ones (Mf and Mm), provided in a global grid of 1440 x 721 points, at 0.25º spatial resolution (http://volkov.oce.orst.edu/tides/global.html). These components were used to reconstruct the hourly AT series since 1948. Results were validated using the area tidal gauges (see Figure 2) with root mean square errors of less than 0.2 cm (at macro-tidal regimes, lower in micro-tidal sites), so that reconstruction of the AT can be considered adequate for offshore depths. The distribution of the 90th percentile of AT is shown in Figure 3 (right panel) and the region's great spatial variation is clear, with microtidal regimes in tropical latitudes, and macrotidal ones in the south.

Storm surge was obtained numerically using the Regional Ocean Modeling System (ROMS) (Shchepetkin and MacWilliams, 2003) at 0.25ºx0.25º resolution, from 125ºW to 20ºW longitude and 61ºS to 40ºN latitude. We used the inverse barometer condition and obtained atmospheric forcing (pressure and wind data) from NCEP/NCAR reanalysis (Kalnay et al., 1996), resulting in hourly time series of storm surge in the period from 1948 to 2008. These results were validated with instrumental tidal gauge data. Figure 2 shows the results of the validation for several tidal gauges in the zone. A good fit for both the statistical distribution and surge time series (not shown) has been obtained. The panels show the scatter, quantile-quantile plot, and statistical diagnostic indices of observed versus modeled data. Colors indicate the sample density. The solid line corresponds to y = x (Modeled equal to Observed data). White diamonds show quantiles higher than 90th percentile. We also show the data number in the dataset (NObs), the BIAS (mean(y) – mean (x)), RMSE (the root mean square error) and the Pearson's correlation coefficient (CORR). It should be noted that this dataset does not include hurricanes, which define the SS extremes tail, because of the insufficient wind and pressure resolution of the NCEP/NCAR reanalysis. An accurate definition of hurricanes requires a specific analysis which is not included in this work without loss of generality for the results in the region covered.

In Figure 3 (left) the storm surge 99th percentile along the coast under study is presented. A large spatial variation in SS can be seen throughout the region. The highest values (over 1 m) are clearly found in the Río de la Plata area, a shallow platform where water accumulates during storm events. In general, the highest values are found in the southern part of the continent, particularly along the Atlantic coast. On the Pacific coast, north of the 35º S parallel, the storm surge of the 99% percentile is about 10 cm almost throughout the whole region, except in areas like the Gulf of California and the Colombian coast, where higher values are found. In this regard, it must be emphasized that local amplifications due to coastal zone local geometry and bathymetry demand greater spatial resolution, which is beyond the scope of this study.

By aggregating the components of AT and SS to the MSL series, it is possible to reconstruct the TSL series, as shown in Figure 4 for two specific points in the region. A first point is on the Chilean coast, where a semidiurnal tidal pattern is dominant, while the second one is found on the Caribbean coast, where tides are mixed and the tidal range is smaller. The weight of each component at each location differs clearly. This aspect is analyzed in section 3.3, along with the comparison with the SLR trends.

3.2. Statistical methods

3.2.1. Long-term trends

The long-term variability of geophysical variables is generally described by calculating regional trends or using global averages. Trends have been detected using both linear and non-linear methods for several variables, even with discontinuous datasets (e.g., Jevrejeva et al., 2006; Barbosa, 2008; Barbosa and Andersen, 2009; Gazeaux et al., 2011; Church et al., 2010). However, such methods only consider the temporal structure missing the spatial influence on them when estimating trends, generally. Moreover, trends detection is sensitive to the record length and the variance of the signal, among some other factors (see Weatherhead et al., 1998; Weatherhead et al., 2002; Whiteman et al., 2011). Thus the influence of phenomena such as ENSO must be taken into account *a priori* as they may affect the calculation of the trend (Lawrence et al. 2004; Becker et al. 2012).

Attempts to overcome these difficulties use techniques based on Empirical Orthogonal Functions (EOF; Fukuoka, 1951), by decomposing a continuous space-time field into an optimal set of basis functions of space and expansion functions of time. However conventional EOF analysis is in general, and among other difficulties, unable to find trends (Hannachi, 2007) since a substantial part of the signal variance is distributed into the different spatial-temporal modes. Hanachi (2007) found a modification of traditional EOF analysis to overcome this limitation (henceforth Trend-EOF).

The method is based on an eigen-analysis of the covariance matrix, similar to conventional EOFs, but taking the time positions of the sorted observations (named as inverted ranks) instead of the direct observations. The different sequences of inverse ranks provide a robust measure of monotonicity. Therefore, maximization of monotonicity can be obtained from maximization of the variance of a linear combination of the inverse ranks, ultimately leading to the identification of robust spatial-temporal trend patterns. This technique has already been used successfully for other geophysical variables (see Barbosa and Andersen, 2009).

In this work, the Trend-EOF technique was used to determine past changes in regional MSL and to compare the results with those obtained by linear regression of the time series. The hypothesis testing related to linear regression results were evaluated by a *t*-test.

3.2.2. Extreme value analysis

Statistical modeling of extreme values requires the use of the extreme value theory, which provides a different approach than that of the mean value statistics. In the context of extreme values, it is necessary to model the mean, the variance and the shape of the distribution. The statistical model proposed for this study is based on a generalized extreme value (GEV) distribution. The GEV model works with a sample of maximum values from blocks of equal temporal length. We defined the block span as a month, which provides a better description of extreme sea-level events within a year, allowing us to analyze the seasonal scale of interest. These maxima blocks are often assumed to be independent and identically distributed random variables, but natural climate variability induces changes in the monthly maxima. This fact contradicts the hypothesis of homogeneity through consecutive months. Therefore a non-stationary approach was used. We considered a time-dependent extreme model characterized by time-dependent location $\mu(t)$ and $\psi(t)$ scale parameters of the GEV distribution. The GEV cumulative distribution function of a certain random variable, Z_t, is given by:

$$F_t(z) = \begin{cases} \exp\left\{ -\left[1+\xi\left(\frac{z-\mu(t)}{\psi(t)} \right) \right]_+^{-1/\xi} \right\} & \xi \neq 0 \\ \exp\left\{ -\exp\left[-\left(\frac{z-\mu(t)}{\psi(t)} \right) \right] \right\} & \xi = 0 \end{cases} \quad (1)$$

where $[a]_+ = \max[a,0]$ and ξ is the shape parameter which informs us about the tail of the distribution. The GEV distribution includes three distribution families corresponding to the three different types of tail behavior: (1) the Gumbel family ($\xi = 0$) characterized by a light tail decaying exponentially; (2) the Fréchet distribution, where $\xi > 0$ and a heavy tail decays polynomially; and (3) the Weibull family, where $\xi < 0$, characterized by a bounded tail. This version of the GEV distribution has been recently used for different geophysical variables (Katz, 2002; Méndez et al., 2007; Menéndez et al., 2009; Rust et al., 2009; Izaguirre et al., 2010; Menéndez and Woodworth, 2010).

Mean sea-level seasonal oscillations have been widely studied (e.g., Tsimplis and Woodworth, 1994) and at a continental scale they are presumed to differ greatly among locations. In this approach, seasonal variability was explicitly modeled by allowing annual and semiannual cycles in location and scale parameters. Menéndez and Woodworth (2010) studied extreme sea-level events from a global dataset of tidal gauges using this approach with successful results. They found the simplest model with a minimum number of time-dependent parameters through a stepwise procedure evaluating the final prediction error criterion (Menéndez et al., 2009; Mínguez et al., 2010a). These methods provide an automatic way of parameter selection which minimizes the Akaike Information Criterion (AIC). Incorporation of additional parameters at every iteration is based on sensitivity analysis and score test statistical information. The methods have proved to be efficient and robust, obtaining the best possible parameterization automatically.

Therefore, only significant sinusoidal functions (at 95% confidence levels) are included in the optimal model for each location (see Menéndez et al., 2009 and Minguez et al., 2010a for further details). The model used for the study of monthly TSL maxima follows:

$$\begin{aligned}
\mu(t) &= \beta_0 + \sum_{1}^{2}\left(\beta_{2i-1}\cos(i\omega t) + \beta_{2i}\sin(i\omega t)\right) + \beta_{LT}\cdot t \\
\psi(t) &= \alpha_0 + \sum_{1}^{2}\left(\alpha_{2i-1}\cos(i\omega t) + \alpha_{2i}\sin(i\omega t)\right) + \alpha_{LT}\cdot t \\
\xi(t) &= \xi_0 + \sum_{1}^{2}\left(\xi_{2i-1}\cos(i\omega t) + \xi_{2i}\sin(i\omega t)\right)
\end{aligned} \qquad (2)$$

where β_0 and α_0 are mean values, β_i and α_i are the amplitudes of the harmonics, $\omega = 2\pi$ year^{-1} and t is given in years. Thus stated, the model is able to simulate the increase or decrease, not only in the magnitude of the extreme events, but also in their variance. The significance of each linear trend was computed using the likelihood ratio test.

To determine whether the SS showed different trend behavior within seasons, the model was modified by including the annual cycle in the term accounting for the long-term trend in the location parameter. The resultant model is expressed as:

$$\begin{aligned}
\mu(t) &= \beta_0 + \sum_{1}^{2}\left(\beta_{2i-1}\cos(i\omega t) + \beta_{2i}\sin(i\omega t)\right) + \left[\beta_{LT} + \beta_{LT1}\cos(\omega t) + \beta_{LT2}\sin(\omega t)\right]\cdot t \\
\psi(t) &= \alpha_0 + \sum_{1}^{2}\left(\alpha_{2i-1}\cos(i\omega t) + \alpha_{2i}\sin(i\omega t)\right) + \alpha_{LT}\cdot t \\
\xi(t) &= \xi_0 + \sum_{1}^{2}\left(\xi_{2i-1}\cos(i\omega t) + \xi_{2i}\sin(i\omega t)\right)
\end{aligned} \tag{3}$$

where β_{LT1} and β_{LT2} represent the amplitudes of the harmonics for the seasonal trends.

Extreme analysis of TSL (equation 2) and SS (equation 3) time series was performed applying the above methods, respectively. To report extreme value intensity we chose a quantile of probability distribution, linked to a 50 year return level, which corresponds to a given no-exceedance probability of $1-q$, with $q = 1/50$. It was obtained for each season by iteratively solving:

$$1-q = \exp\left\{-k_m \int_{t_a}^{t_b}\left[1+\xi(t)\left(\frac{\overline{z}_q[t_1,t_2]-\mu(t)}{\psi(t)}\right)\right]_+^{-1/\xi(t)} dt\right\} \tag{4}$$

where $[t_a, t_b]$ is the interval equal to one season and $1/k_m$ is the length of the block maxima, that is, one season (3 months) so that $1/k_m = 1/4$ year. Details regarding the derivation of equation (3) can be found in Frías et al. (2011).

4. STUDY OF SEA-LEVEL COMPONENTS

4.1. Changes in Mean Sea-Level

Two trend techniques have been used to study sea-level globally: the Trend-EOF and a trend based on linear regression on local time series. In both cases we used two regression models: a first ($z = at + b$) and a second ($z = at^2 + bt + c$) grade models.

Assessment of the minimum quadratic error, proved the regression by both methods to be quadratic. This result suggests a mild acceleration of trends in the period 1950-2008. Figure 5 shows the time series for average global sea level and the first component of the Trend-EOF (i.e. that including the trend's global pattern), with a value of 2.7 mm/yr in 2010 and a 0.01 mm/yr^2 curvature. The statistical significance of our results was higher than 95%, and they are in accordance with previous trends calculated for mean global sea level (e.g., Church et al., 2004; Church et al., 2010; Cazenave and Remy, 2011; Becker et al., 2012; Meyssignac and Cazenave, 2012).

Because of the importance of interannual sea-level variability, the Trend-EOF technique is probably more adequate for spatial analysis of trends, since it is not influenced by local effects and hence, it maintains spatial homogeneity. Figure 6 shows the results of global patterns in the average trend calculated by Trend-EOF and local regression in the study region.

The trend is unmistakably for the mean sea-level to rise at all points in the region, as shown in the various time series panels in Figure 7. The highest values for these trends are found on the Atlantic coast, approximately 2 mm/yr on the northern coast of South America and the Caribbean coast, with lower values on the Caribbean islands. In the equatorial Pacific area the increase is lower (1-1.5 mm/yr). In addition, the influence of the ENSO phenomenon (periods of el Niño and la Niña) is seen in the time series of anomalies, particularly along the Pacific coast, as will be analyzed in section 4.

At this point it is worth comparing the effect of climatic variability on MSL over a multiple-year time scale, and the current long-term trend maintained in recent decades. Figure 7 shows the different influence of el-Niño and la-Niña events on the Pacific coast of Central America, from Mexico to the coast of Peru. In 1998 (the Niño3 index historical high), the el-Niño index's greatest influence occurred in the equatorial zone of the Pacific (not shown spatially but identified in Figure 7 at point 598). If the sea-level time series are detrended, it becomes possible to determine the scale of this event on MSL. A similar event would give values of around 20 cm at the point of maximum effect (considering only the effect on MSL and not the accumulated effects on other variables such as wave climate (see Reguero et al., 2012b) or SS. This highlights the importance of studying all TSL components to discern the relative weight of changes to each component.

4.2. Changes in extreme storm surge levels

Extreme storm surge events decisively influence coastal flooding, making it essential to analyze them and their trends. An analysis of extremes of Storm Surges was performed, based on GEV distribution and applied to the monthly maxima (see equation 3) over the period from 1948 to 2008, making it possible to determine significant seasonal trends.. Seasons were organized into three-month blocks: December, January, February (DJF); March, April, May (MAM); June, July, August (JJA); and September, October, November (SON). Hurricanes were not included in the data base because of the lack of resolution in the pressure and wind fields in NCEP/NCAR reanalysis. Thus analysis in Central America and the Caribbean must be treated with caution because the magnitude of extreme values is not well represented, as the SS distribution tail is defined by these hurricane events.

Figure 8 shows SS over a 50 year return period. The highest values are found at the Río de la Plata with a surge height of more than 3 m, diminishing northward and southward. This area has one of the largest AT and the greatest average SS level, so MSL changes are insignificant in proportion to SS and tidal range.

Figure 9 depicts the annual trends for the SS extremes (central panel), where only results over the 95% statistical significance level are shown. Seasonal behavior is also incorporated at certain representative points in the Figure. The results indicate that the zone with the greatest positive trend was that of Río de la Plata, with values of up to 5 mm/yr between 1948 and 2008. This was also the area with the greatest surge extremes, throughout all seasons. Trends decrease to 2 mm/yr immediately southwards from the river inlet and reaching the southern Brazilian coast northwards. These results are in accordance with those in Fiore et al. (2009) who found seasonal increase in frequency of SS events and long-term trends of 2 mm/yr from Mar de Plata tidal gauge. Remarkable negative trend was found in the Gulf of California where it is reduced at approximately 3 mm/year, with a marked seasonality, dropping particularly during the occurrence of Northern Hemisphere winters (DJF). A moderate (1.5 mm/yr) increase in surge extremes was noted on the southern Brazilian coast along with a similar reduction in the northern one. Seasonality was also marked in this zone. On the other coasts in the study area, trends were less than 1 mm/yr, either increasing or decreasing, although always significant. No significant differences in extreme values were detected in the area affected by hurricanes and tropical storms, although this result cannot be conclusive because the magnitude of the hurricane peaks is not well-represented in our analysis.

4.3. Relative influence of sea-level components

By aggregating the sea-level components, Figure 10 shows the relative importance of each TSL contributors at various points. The panels on the left show the probability density functions (pdf) of AT, SS and TSL, while those on the right show the mean MSL seasonal range and the pdf of the MSL value in 2030 by extrapolating the calculated trends. These were designed to identify the proportion of the long-term change with respect to the seasonality, assuming that the acceleration observed until now remains constant. The average regression estimator in the target year (2030) was obtained, to extrapolate the SLR value.

As shown in this figure, the AT dominates in general the TSL pdf except when the SS variation range is such that it surmounts astronomical influences, which only occurs in the Río de la Plata (point 384 in the Figure). At the remaining locations, the SS variation range is below that of the AT, irrespective of tidal range (Figure 10).

MSL seasonality also shifts spatially (between 12 and 4 cm on average), in proportion to the long-term trends. In areas where this seasonality is small (the tropical Atlantic coast and the south Pacific) SLR takes on greater importance. However, in macrotidal regions, because of the wide AT variation, the proportion of change due to SLR is marginal, i.e.: around 2.5% of change in the TSL range at point 1123 in southern Chile.

4.4. Changes in extreme total mean sea-levels

Results reveal that the coefficients in the location and scale parameters accounting for a long-term variation are significant for most of the points under study (maps in Figure 11). The variation of the location parameter implies a shift in the average of the TSL pdf while the scale parameter change is related to a modification of its variance. The subsequent effect of the TSL pdfs varying in time (from 1950 to 2008) can be clearly detected in Figure 11. Spatially, the pattern of trends reveals a large variability.

In general, trends in sea-level extremes (Figure 11) rise by up to 7 mm/yr in the Río de la Plata area, in line with previously estimated MSL trends and SS extremes. Elsewhere in the region, trends ease to 2 mm/yr, with the MSL contributing predominantly over higher SS. A slight reduction is noted in the Gulf of California, induced by negative trends in SS extremes.

Figure 11 shows pdf variations in 5 year periods since 1950 at various representative locations. At sites with a long-term trend in the parameter of scale (e.g. point 1005) the pdf widens, making extreme values the most likely. At other points, particularly on the Atlantic coast, the trend in the parameter of scale was negligible (see the upper panels in Figure 12), so that the pdf shift is driven solely by the trend in the shape parameter. Extreme values were also more frequent in these cases.

There were, nevertheless, points where no significant trends were found, neither in the scale nor in the location parameters, such as for example on the coast of Ecuador (i.e. Id. 620, Figure 12). To provide a further insight into it, Figure 12 shows the temporal series of monthly maxima and the results of the adjusted parameters for two example points. In some cases (the top panels in Figure 12) no significant long-term trends in extreme pdf parameters were found. Yet at other points (lower panels in the figure) this trend was significant for one or several parameters.

Long-term shifts in extreme pdfs suggest that extreme values have become more frequent in recent decades. This was quantified by obtaining extreme TSL values with a return period of 100 years in two specific periods, during the first 10 years of available data (1950-1960) and during the last 10 years of analysis (1998-2008). The difference is shown in Figure 13. The panel on the left reveals the increase associated with the 100-year return period level, at its greatest in northern Argentina, Uruguay and southern Brazil, where the trend is dominated by SS extremes. At the remaining points, the MSL trend predominates and the change is not so obvious. However, if these differences are expressed in proportion to the value for the average return period between 1950 and 1960, the Caribbean islands saw this extreme value increase by more than 60% during that decade, compared with the 1998-2008 one (with the aforementioned caution that hurricanes are not properly modeled in the peak magnitude of SS events).

These results imply that coastal flooding risk in low-lying areas may be increasing due to a combination of rising MSL and variations in SS extreme events. By itself, rising MSL may not cause flooding but, a rising water level has caused a decrease in the return periods of the extreme total water levels during the last five decades (Figure 13). The proportion of these changes with respect to current dynamics (Figure 10) will play an important role in impact evaluation and adaptation strategies.

5. Discussion of climate variability influence

As already seen in the MSL series, interannual variability arising from the ENSO phenomenon is in some cases clearly marked. Indeed, the ENSO phenomenon is known to have an effect on sea-level in the Pacific Ocean (e.g., Walsh et al., 2012; Liu et al., 2009). Should changes in this climatic pattern occur (Collins et al., 2010) they will in turn influence sea-levels (Church et al., 2006; Lowe et al., 2010).

To analyze the influence of various climate patterns in sea-level components in the region of study a number of climatic indices were considered: the Arctic oscillation (AO), the Southern Annular oscillation (SAM), the ENSO measured through the Niño3 index and the Southern Oscillation Index (SOI), the Pacific North American Index pattern (PNA), the Western Pacific Index (WP), the Eastern Pacific Oscillation (EP/NP), the Caribbean Sea Surface Temperature Index (CAR), Northeast Brazil rainfall (NBR), the North Tropical Atlantic Surface Temperature Index (NTA), the Tropical North Atlantic Index (TNA), and the Tropical Southern Atlantic Index (TSA). A comprehensive list with definitions, descriptions and references can be found at http://www.esrl.noaa.gov/psd/data/climateindices/list/. The standardized series of the different climatic indices was correlated with the MSL and the 95th percentile of SS. Figure 14 shows the Pearson correlation coefficients (varying between -1 and +1) at the points were correlation was significant at least at the 95% confidence level. A cross correlation analysis was also performed (not shown) to identify patterns whose influence may be deferred in time between the value of the climatic index and the maximum effect on sea-level on the coasts in the region of study.

Figure 14 shows the correlation coefficient of the Niño3 climatic index with the normalized variables: MSL and the 95th percentile of SS. Niño3 showed the greatest correlation on sea-level components, as can be seen in the temporal series in Figure 7, with a virtually simultaneous correlation with them (with no time lag). The Niño3 index has a high correlation (correlation > 0.5), with standardized anomaly of MSL on the Pacific coast, between 15ºS and 30ºS on the Atlantic, and on the Caribbean islands. On the rest of region, the correlation was still positive but with lower values. Thus, Niño3 led to a generalized rise of sea-level throughout the study area, particularly on the continent's Pacific coast. Other indices such as TNA, CAR and AMO (not shown) also influenced sea-level anomalies significantly, although their correlations were lower.

Storm surge showed a correlation with Niño3 of 0.2, for the entire Pacific coast. Positive values of this index are found to be related to a general rise in SS along the continent's Pacific façade, including the Caribbean islands and reaching the Gulf of Mexico where the correlation turns negative. On the Pacific coast, positive correlations are found west of the California peninsula and southwards while the correlation becomes negative in the Gulf of California. Slightly negative values appear on parts of the tropical Atlantic coasts and Argentina. Concerning other indices (not shown), the influence of the NTA index is found to be positive on the Caribbean islands, and TSA is associated with negative rises between 15ºN and 15ºS on the Atlantic coast and in the Gulf of California.

In view of the correlation pattern, an insight on the relationship between the Niño3 and the MSL must be carried out. To determine the contribution of the Niño3 climate index to MSL, a simple regression model was built for the various points analyzed in the region. The results (shown in Figure 15 for a representative point in the Peruvian coast) show a clear relationship (panel b in the Figure 15) with the mean estimate of: MSL (mm) = 30.47 x Niño3*, where Niño3* represents the standardized climate index time series on a monthly scale. This simple model explains over 65% of the variance in MSL data (panel a). The mean estimate corresponds to over 30 mm per unit of standardized index in a great part of the region (panel c), from 15ºS to 15ºN. The effect of Niño3 in the rest of the region is residual which may be indicating that a combination of climate patterns is occurring there.

6. Conclusions

This work provides a description of the various components of sea-level by constructing and analyzing time series of Astronomical Tide, Storm Surges and Mean Sea-Levels using different databases (both instrumental and numerical), for the region of Latin America and the Caribbean (LAC). In particular the Storm Surge reanalysis performed at a 0.25º spatial resolution in the study area must be highlighted. However, it has to be noted that this contribution does not include an adequate description of hurricane events in the Caribbean due to insufficient resolution in the forcing fields (taken from NCEP/NCAR reanalysis). With this in mind, within the period from 1950 to 2008 Storm Surge heights were largest in the area of Rio de la Plata, while the greatest Astronomical Tides occur in southern latitudes of the continent and in the Gulf of California.

The results here obtained are believed to provide useful insights in the determination of the probability of flooding in the coastal areas of Latin America and the Caribbean and they may also constitute an adequate approach for other areas of the world. As seen in this work, the variables contributing to total sea-level at each particular coast reveal different importance. Pinpointing the dominant variables, their changes and their aggregated effect on coastal flooding is thus crucial in order to lead efforts to its prevention and management.

With respect to the relative weight of each component on sea-level, certain features need to be highlighted. Past changes in sea-level present a higher weight in the Caribbean Islands in relation with the low range of tidal variability. This occurs together with a tail of distribution dominated by extreme events and associated with tropical storms and hurricanes. Despite the low rates of change detected and considering that modeling must be taken with caution, extremes seems to have increased considerably in intensity during the last 5 decades, showing a special sensitivity of this area to low rises in water levels. This, together with the particular social, environmental and economic characteristics of the coastal zones in the islands should be a matter of concern and needs further research. The trends in water levels found here are negligible in comparison with the tidal ranges and the storm surge heights registered at extra-tropical areas. In these areas, flooding may be induced by changes in the storm surge regime, as a result of variations in the storm activity of the southern hemisphere, and coinciding with high tides. A remarkable exception is the Río de la Plata area where storm surge surpasses the tidal range, future changes in this component being one of the major hazards for coastal zones in the area.

Owing to inter-annual changes in the region, like the ENSO phenomenon, which significantly affect certain areas of the LAC coasts, long-term trends in Mean Sea-Level data were computed using two different techniques: local regression and the Trend-EOF technique. Results were similar for most of the study area and in accordance with previous works at a global scale. However, the Trend-EOF approach provides a more uniform estimate for the whole region while revealing a lower trend in the tropical Pacific coast, which was also the case with local regression.

Storm surge monthly maxima were analyzed with a non-stationary extreme value model based on a GEV distribution accounting for long-term trends in location and scale parameters. Increase of Storm Surge of around 5 mm/yr were found in the Rio de la Plata margin, precisely where Storm Surge events are of greatest concern.

Building hourly time series of Total Sea-Level in the period from 1950 to 2008 by aggregation of the three components, the resulting data were analyzed with the non-stationary extreme analysis approach to identify long-term trends, which varied on average from 2 to 7 mm/yr. The quantile associated with a 50-yr return period was then computed to find that it has been changing during the last decades due to modifications in probability density functions, which were variable spatially. Larger relative changes may be occurring in the southern Caribbean, notwithstanding the fact that the hurricane tail of the distribution is not properly modeled in this analysis and that the largest changes in magnitude are found in the Rio de la Plata area. Indeed, up to 7 mm/yr were detected in storm surge past events in Rio de la Plata because of a clear translation in the mean value of the extreme probability density function. Meanwhile, at the Caribbean the probability density function of extremes of total sea-level are widening and translating, leading to higher probability for extremes.

El-Niño events are widely known to influence sea-levels in the Pacific Ocean. The highest historical event (1989) was in the same order of magnitude as the long-term change in Mean Sea-Level detected over the last 6 decades in the study region. This sets off the effects that variations in the ENSO phenomenon could entail as suggested by recent studies. In fact, a clear correspondence was found through a simple regression model between Mean Sea-Level and the Niño3 climate index, which in turn explained more than 65% of the variance in the signal and seemed to have an effect of over 30 mm per unit of standardized index in the tropical Pacific coast of LAC. The high tail of the Storm Surge distribution seems also to be related to this and other climatic patterns but its assessment falls out of the scope of this work and was hence not evaluated.

Acknowledgements

The authors wish to acknowledge the NOAA - National Weather Service and the British Antarctic Survey for providing data on climate indices. The altimeter data were produced and distributed by AVISO (http://www.aviso.ocanobs.com/). B.G. Reguero is indebted to the University of Cantabria for funding. This work was partly funded by projects 'GRACCIE' (CSD2007-00067, Programa Consolider-Ingenio 2010) and ‘IMAR21’ (CTM201015009) from Spanish Ministries of Economy and Agriculture, Food and Environment.

This work was part of the “R*egional study on the effects of Climate Change in the coast of Latin America and the Caribbean*” supported by the Economical Commission for Latin America and the Caribbean (ECLAC) from the United Nations (UN) and the Spanish Agency on Climate Change (OECC).

REFERENCES

Ardalan A.A., Hashemi-Farahani, H. 2007 A harmonic approach to global ocean tide analysis based on TOPEX/POSEIDON satellite. Marine Geophysical Research, 28, 235-255.

Akaike, H. 1973 Information theory and an extension of the maximum likelihood principle. In: Proceedings of the 2nd International Symposium on Information Theory, edited by B. N. Petrov and F. Csáki, pp. 267–281, Akadémia Kiadó, Budapest.

Barbosa, S. M. 2008 Quantile trends in Baltic sea level, Geophysical Research Letters, 35, L22704, Doi: 10.1029/2008GL035182.

Barbosa, SM, Andersen, OB, 2009 Trend patterns in global sea surface temperature. International Journal of Climatology, DOI: 10.1002/joc.1855

Cazenave, A., Lombard, A., Llovel, W. 2008 Present-day sea-level rise: A synthesis. Oceanography. C.R. Geoscience, 340, 761-770.

Cazenave, A., Remy, F. 2011 Sea-level and climate: measurements and causes of changes. WIREs Climate Change, 2: 647–662. Doi: 10.1002/wcc.139

Church, J.A., White, N.J., Coleman, R., Lambeck, K., Mitrovica, J.X. 2004 Estimates of the regional distribution of sea-level rise over the 1950 to 2000 period. Journal of Climate, 17, 2609-2625.

Church, J.A., White, N.J., Hunter, J.R. 2006 Sea-level rise at tropical Pacific and Indian Ocean islands. Global and Planetary Change, 53, pp. 155–168. Doi: 10.1016/j.gloplacha.2006.04.001

Church, J. A., Aarup, T., Woodworth, P. L., Wilson, W. S., Nicholls, R. J., Rayner, R., Lambeck, K., Mitchum, G. T., Steffen, K., Cazenave, A., Blewitt, G., Mitrovica, J. X. and Lowe, J. A. 2010. Sea-Level Rise and Variability: Synthesis and Outlook for the Future. In: Understanding Sea-Level Rise and Variability (eds J. A. Church, P. L. Woodworth, T. Aarup and W. S. Wilson), Wiley-Blackwell, Oxford, UK. Doi: 10.1002/9781444323276.ch13

Collins, M., An, S.I., Cai, W., Ganachaud, A., Guilyardi, E., Jin, F.-F., Jochum, M., Lengaigne, M., Power, S., Timmermann, A., Vecchi, G., Wittenberg, A. 2010 The impact of global warming on the tropical Pacific Ocean and El Niño. Nature Geoscience, 3, pp. 391–397. Doi: 10.1038/ngeo868

Dasgupta, S., Laplante, B., Murray, S., Wheeler, D. 2009 Sea-Level Rise and Storm Surges: A Comparative Analysis of Impacts in Developing Countries. The World Bank, Development Research Group - Environment and Energy Team. Policy Research working paper nº 4901

De Santis, A., Qamili, E., Spada, G., Gasperini, P. 2012 Geomagnetic South Atlantic anomaly and global sea-level rise: A direct connection? Journal of Atmospheric and Solar-Terrestrial Physics, 74, 129-135. Doi: 10.1016/j.jastp.2011.10.015

Egbert G.D., Bennett A.F., Foreman M.G.G. 1994 TOPEX/POSEIDON tides estimated using a global inverse model. Journal of Geophysical Research, 99(C12), 24821-24852.

Egbert G.D., Erofeeva, S.Y., 2002 Efficient inverse modelling of barotropic ocean tides. Journal of Atmospheric and Oceanic Technology, 19, 183-204.

Ericson, J.P., Vorosmarty, C., Dingman, S., Ward, L., Meybeck, M. 2006 Effective sea-level rise and deltas: Causes of change and human dimension implications. Global and Planetary Change 50, 63–82.

Fiore, M.M.E., D'Onofrio, E.E., Pousa, J.L., Schnack, E.J., Bértola, G.R. 2009 Storm surges and coastal impacts at Mar del Plata, Argentina. Continental Shelf Research 29, 14, 1643-1649

Frías, M. D., Mínguez, R., Gutiérrez, J. M., Méndez, F.J. 2011. Future regional projections of extreme temperatures in Europe: A nonstationary seasonal approach. Climatic Change, 1-22. Doi: 10.1007/s10584-011-0351-y.

Gazeaux, J., Flaounas, E., Naveau, P., Hannart, A. 2011 Inferring change points and nonlinear trends in multivariate time series: Application to West African monsoon onset timings estimation. Journal of Geophysical Research, 116, D05101
Doi: 10.1029/2010JD014723.

Hannachi, A. 2007 Pattern hunting in climate: a new method for finding trends in gridded climate data. International Journal of Climatology. 27: 1–15. Doi: 10.1002/joc.1375

Horsburgh, K. J., and Wilson, C. 2007 Tide-surge interaction and its role in the distribution of surge residuals in the North Sea. Journal of Geophysical Research, 112, C08003, Doi:10.1029/2006JC004033.

IPCC (Intergovernmental Panel on Climate Change) 2007. Bindoff, N.L., Willebrand, J., Artale, V., Cazenave, A., Gregory, J., Gulev, S., Hanawa, K., Le Quéré, C., Levitus, S., Nojiri, Y., Shum, C.K., Talley, L.D, Unnikrishnan, A. Observations: oceanic climate change and sea level. In: Solomon, S., Qin, D., Manning, M., Chen, Z., Marquis, M., Averyt, K.B., Tignor, M., Miller, H.L. (Eds.), Climate Change 2007: The Physical Science Basis. Contribution of Working Group I to the Fourth Assessment Report of the Intergovernmental Panel on Climate Change. Cambridge University Press, Cambridge, United Kingdom and New York, NY, USA

Izaguirre, C., Méndez, F.J., Menéndez, M. and Losada, I.J. 2011 Global extreme wave height variability based on satellite data. Geophysical Research Letters, 38 (L10607)

Jevrejeva, S., Grinsted, A., Moore, J.C., Holgate, S. 2006 Nonlinear trends and multiyear cycles in sea-level records, J. Geophysical Research, 111, C09012, Doi:10.1029/2005JC003229.

Kalnay, E., Kanamitsu, M., Cistler, R., Collins, W., Deaven, D., Gandin, L., Iredell, M., Saha, S., White, G., Woolen, J., Zhu, Y., Chelliah, M., Ebisuzaki, W., Higgins, W., Janowiak, J., Mo, K., Ropelewski, C., Wang, J., Leetma, A., Reynolds, R., Jenne, R., Joseph, D. 1996 The NCEP/NCAR reanalysis project. Bulletin of the American Meteorology Society 77, 437-471.

Katz, R.W., Parlange, M.B., Naveau, P., 2002 Statistics of extremes in hydrology. Advances in Water Resources, 25, 1287-1304.

Lawrence, S.P., Llewellyn-Jones, D.T., Smith, S.J. 2004 The measurement of climate change using data from the advanced very high resolution and along track scanning radiometers. Journal of Geophysical Research 109: C08017.

Liu, X., Liu, Y., Guo, L., Rong, Z., Gu, Y., Liu, Y. 2010 Interannual changes of sea-level in the two regions of East China Sea and different responses to ENSO. Global and Planetary Change Vol. 72, 3, Pages 215–226
Doi: 10.1016/j.gloplacha.2010.04.009

Lowe, J.A., Woodworth, P.L., Knutson, T., McDonald, R.E., McInnes, K.L., Woth, K., Storch, H. von, Wolf, J.A., Swail, V., Bernier, N.B., Gulev, S., Horsburgh, K.J., Unnikrishnan, A.S., Hunter, J.R., Weisse, R. 2010 Past and future changes in extreme sea levels and waves. Church, J.A., Woodworth, P.L., Aarup, T., Wilson, W.S. (Eds.), Understanding Sea-Level Rise and Variability, Wiley.

Méndez, F.J., Menéndez, M., Luceño, A., Losada, I.J. 2006 Estimation of the long-term variability of extreme significant wave height using a time-dependent POT model. Journal of Geophysical Research, 111, C07024.

Menéndez, M., Méndez, F.J., Losada, I.J. and Graham, N.E. 2008 Variability of extreme wave heights in the northeast Pacific Ocean based on buoy measurements, Geophysical Research Letters, 35, L22607.

Menéndez, M., F.J. Méndez, C. Izaguirre, A. Luceño, I.J. Losada, 2009 The influence of seasonality on estimating return values of significant wave height. Coastal Engineering, 56(3), 211-219.

Menéndez, M., Woodworth, P. L. 2010 Changes in extreme high water levels based on a quasiglobal tide-gauge data set, Journal of Geophysical Research., 115, C10011, doi:10.1029/2009JC005997.

Meyssignac, B., Cazenave, A., 2012 Sea level: A review of present-day and recent-past changes and variability. J. Geodynamics. Doi:10.1016/j.jog.2012.03.005. In press

Mínguez, R., Méndez, F.J., Izaguirre, C., Menéndez, M., Losada, I.J. 2010a Pseudo-optimal parameter selection of non-stationary generalized extreme value models for environmental variables. Environmental Modelling & Software 25, 1592-1607.

Nicholls, R.J. 2004 Coastal flooding and wetland loss in the 21st century: changes under the SRES climate and socio-economic scenarios. Global Environmental Change 14, 69-86.

Nicholls, R.J. et al., in Climate Change 2007: Impacts, Adaptation and Vulnerability. Contribution of Working Group II to the Fourth Assessment Report of the Intergovermental Panel on Climate Change, M. L. Parry et al., Eds. (Cambridge Univ. Press, Cambridge, 2007).

Nicholls, R.J., Cazenave, A. 2010 Sea-level rise and its impact on coastal zones. Science. 328, 1517-1520. Doi: 10.1126/science.1185782

Nicholls, R.J. 2011 Planning for the impacts of sea-level rise. Oceanography 24 (2):144–157, doi:10.5670/oceanog.2011.34.

Reguero, B.G., Menéndez, M., Méndez, F.J., Mínguez, R., Losada, I.J. 2012. A global Ocean Wave (GOW) calibrated reanalysis from 1948 onwards. Coastal Engineering, 65, 38-55. Doi:10.1016/j.coastaleng.2012.03.003

Reguero, B.G., Méndez, F.J., Losada, I.J. 2012b. Variability of multivariate wave climate in Latin America and the Caribbean. Global and Planetary Change (in press).

Rignott, E., Velicogna, I., van den Broeke, M.R., Monaghan, A. Lenaerts, J.T.M. 2011.Acceleration of the contribution of the Greenland and Antarctic ice sheets to sea-levelrise. Geophysical Research Letters L05503. Doi: 10.1029/2011GL046583.

Rust HW, D. Maraun, and T.J. Osborn, 2009 Modeling seasonality in extreme precipitation. A UK case study. European Physics Journal, Special Topics, 174, 99–111.

Shchepetkin, A. F. and MacWilliams, J.C. 2003 A method for computing horizontal pressure-gradient force in an oceanic model with a nonaligned vertical coordinate. J. Geophysical Research, 108 (C3), p. 3090, doi:10.1029/2001JC001047

Syvitski, J.P.M., Kettner, A.J., Overeem, I., Hutton. E.W.H., Hannon, M.T., Brakenridge, G.R., Day, J., Vörösmarty, C., Saito, Y., Giosan, L., Nicholls, R.J. 2009 Sinking deltas due to human activities. Nature Geoscience 2, 681 - 686

Tsimplis, M. N., Woodworth, P.L. 1994 The global distribution of the seasonal sea-level cycle calculated from coastal tide gauge data, J. Geophysical Research., 99, 16,031–16,039.

Walsh, K.J.E., McInnes, K.L. and McBride, J.L. 2012 Climate change impacts on tropical cyclones and extreme sea levels in the South Pacific area – A regional assessment. Global and Planetary Change, Vol. 80–81, 149–164.
Doi: 10.1016/j.gloplacha.2011.10.006

Weatherhead, E.C., Reinsel, C., Tiao, G.C., Meng, X., Choi, D., Cheang, W., Keller, T., DeLuisi, J., Wuebbles, D.J., Kerr, J.B., Miller, A.J., Oltmans, S.J. and Frederick, J.E. 1998 Factors affecting the detection of trends: Statistical considerations and applications to environmental data. Journal of Geophysical Research, 103(D14):17149-17161.

Weatherhead, E.C., Stevermer, A.J., Schwartz, B.E. 2002 Detecting environmental changes and trends. Physics and Chemistry of the Earth, Parts A/B/C, Vol. 27, Issues 6–8, 399-403,

Whiteman, D.N., Vermeesch, K.C., Oman, L.D., Weatherhead, E.C. 2011 The relative importance of random error and observation frequency in detecting trends in upper tropospheric water vapor. Journal of Geophysical Research D: Atmospheres, 116 (21), D21118. Doi: 10.1029/2011JD016610

FIGURE CAPTIONS

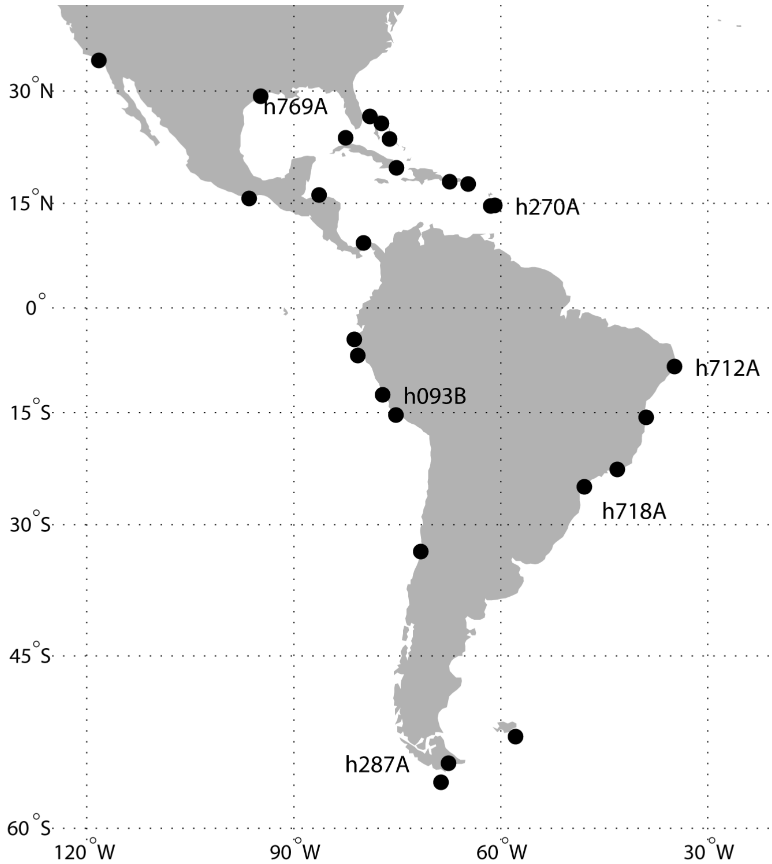

Figure 1. The region of study showing the tidal gauges selected for validation purposes.

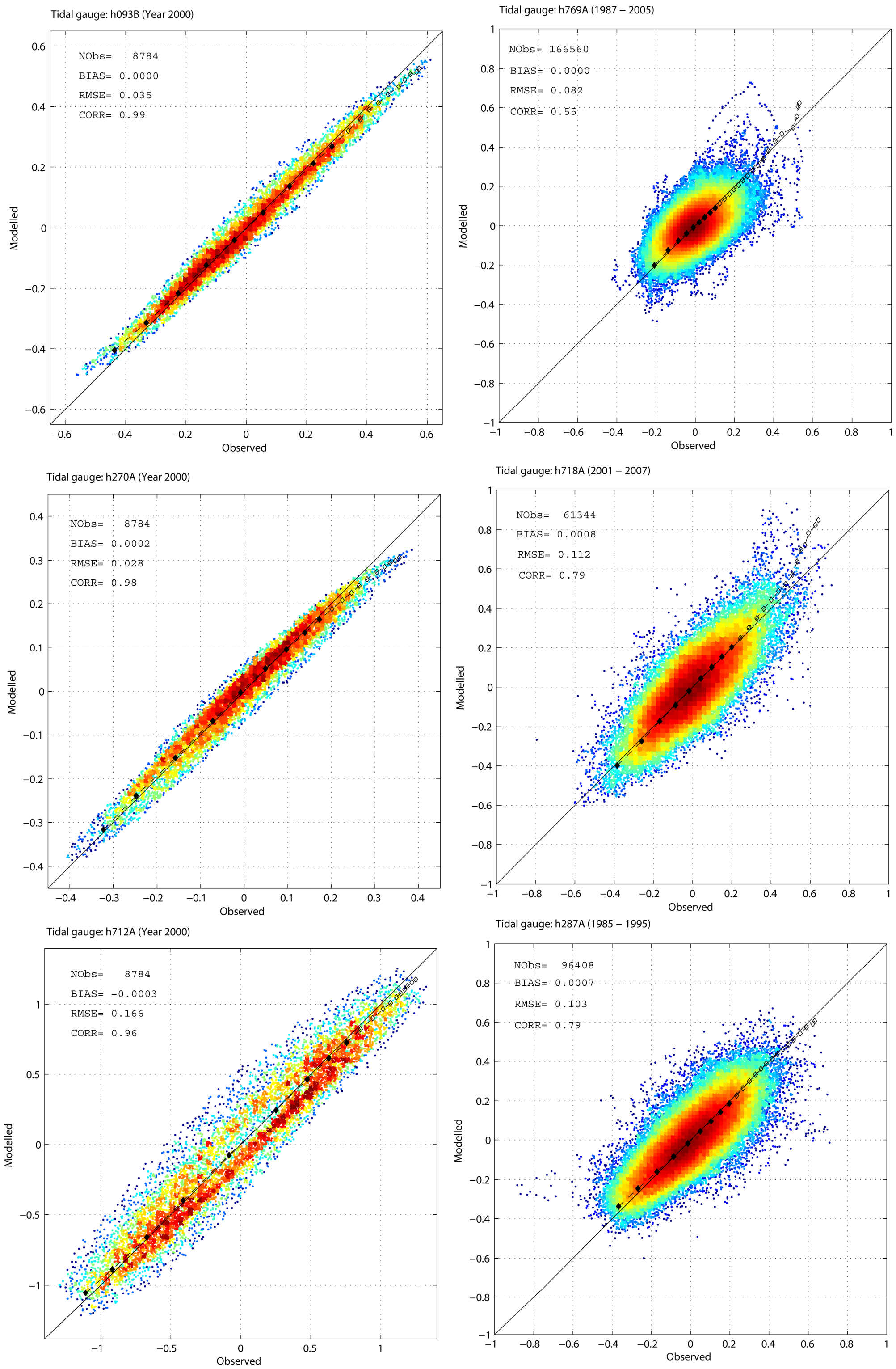

Figure 2. Validation of the reconstruction of the Astronomical Tide (left) and the modeled Storm Surge (right) with various regional tidal gauges in the study area. Scatter data and quantile distribution are shown. Values expressed in meters.

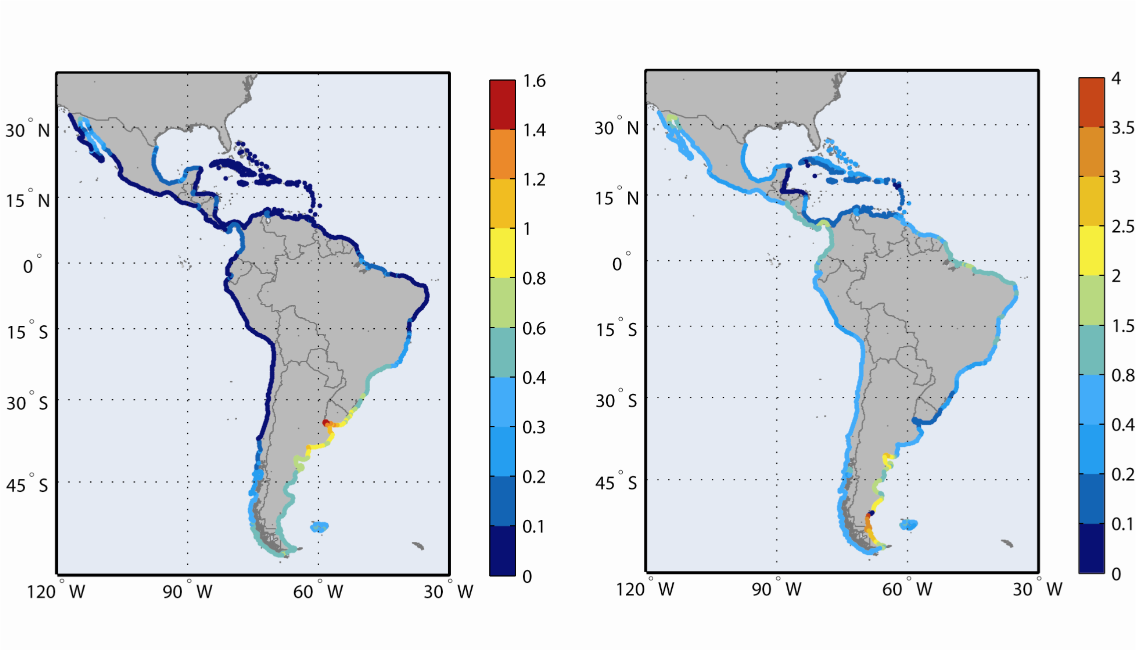

Figure 3. Annual 99% percentile of Storm Surge (left panel) and 90% percentile of Astronomical Tide (right panel), computed for the period 1948 – 2008 and expressed in meters.

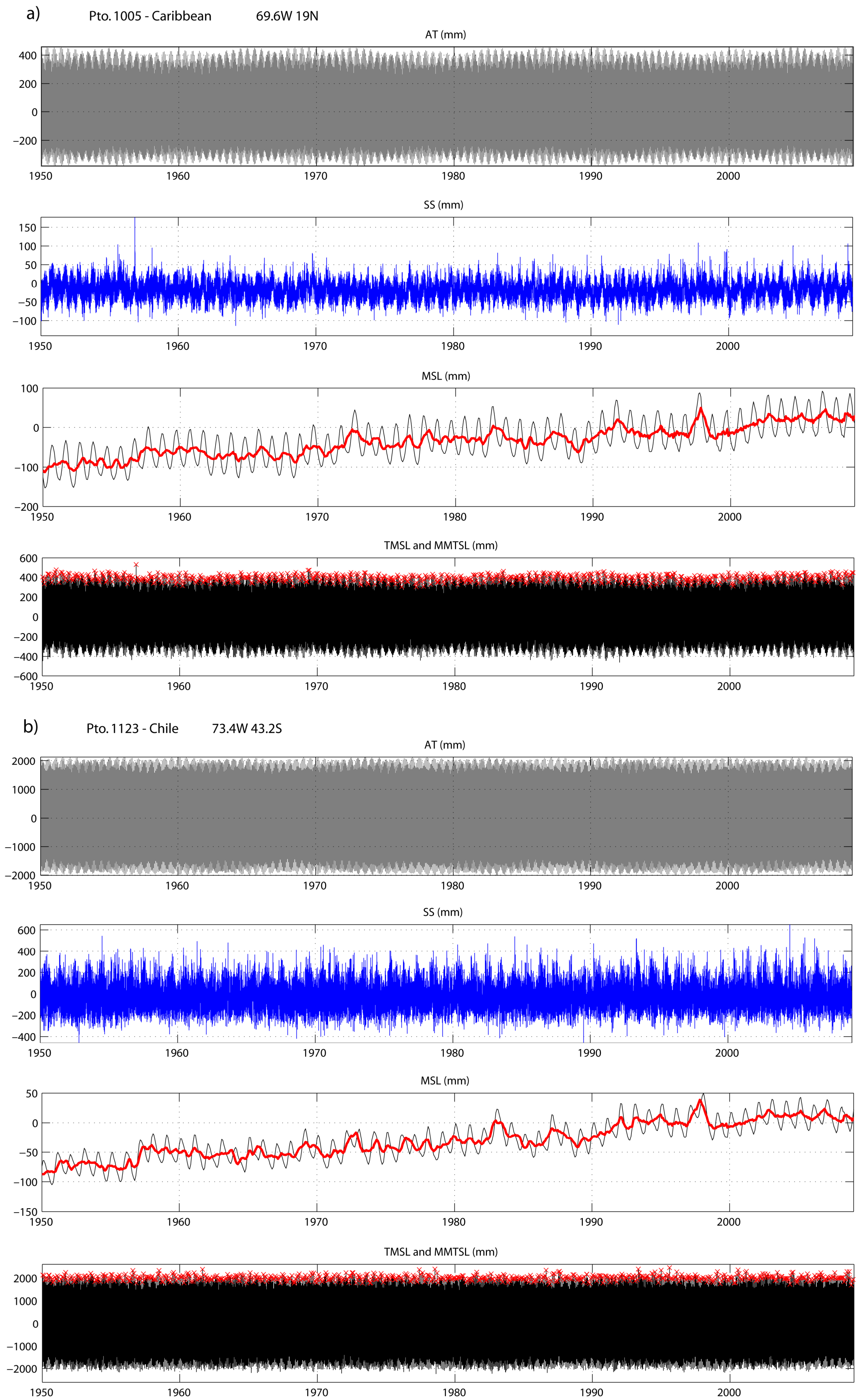
a)
Pto. 1005 - Caribbean
69.6W 19N
AT (mm)
SS (mm)
MSL (mm)
TMSL and MMTSL (mm)
b)
Pto. 1123 - Chile
73.4W 43.2S
AT (mm)
SS (mm)
MSL (mm)
TMSL and MMTSL (mm)

Figure 4. Reconstruction of Total Sea-Level time series (TSL) using the different components at two points in the study region: Caribbean coast (a) and Chilean coast (b). The series are shown for Astronomical Tide (AT), Storm Surge, Mean Sea-Level time series (MSL) and Total Sea-Level (TSL). The red line in MSL represents the annual mean values, while the red-cross line in TSL indicates the Monthly Maxima of Total Mean Sea-Level (MMTSL).

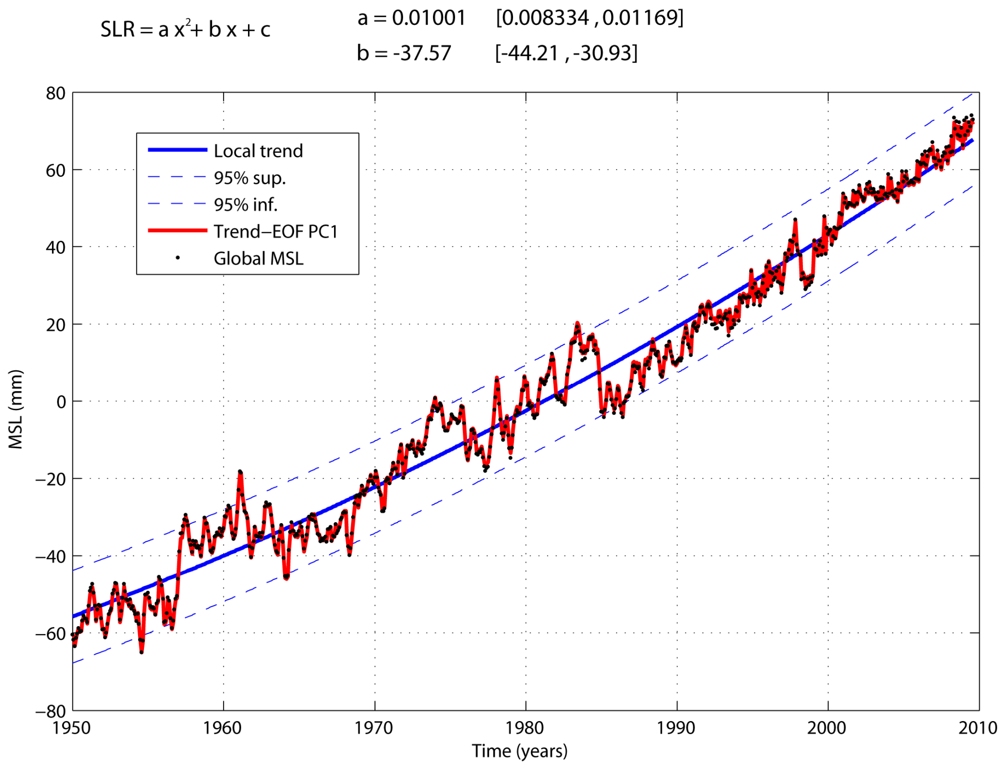

Figure 5. Global mean sea-level trends. Trend derived from the First Trend-EOF component (red) along with the temporal instants of global mean sea-level (black points), trend adjusted with 95% confidence intervals (blue).

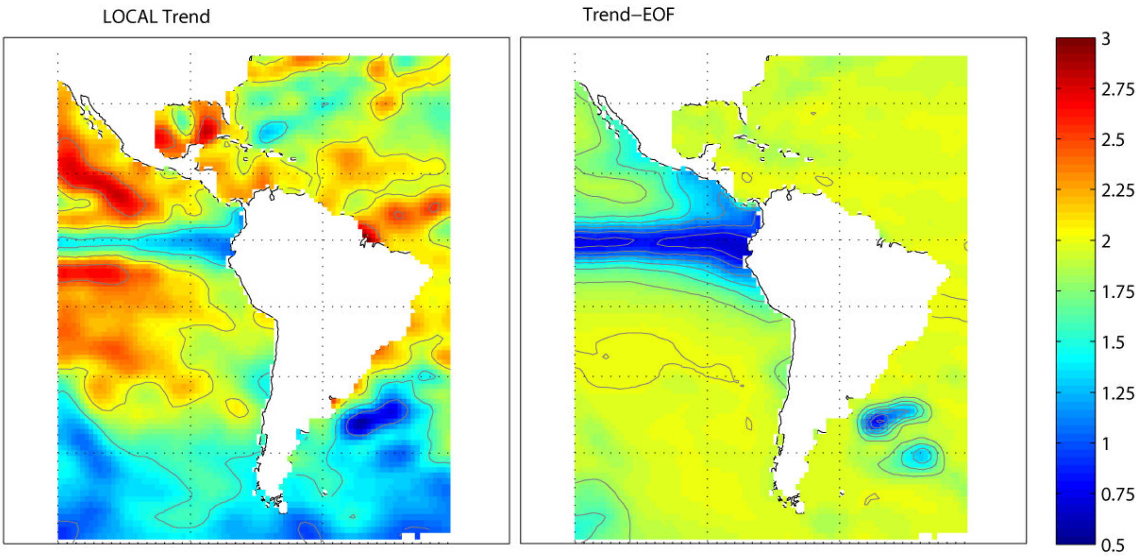

Figure 6. Comparison of the linear trend of rising sea-level obtained by local regression (left) with the one obtained using the Trend-EOF technique (right) for the region of Latin America and the Caribbean (mm/yr). Data analyzed in the period 1950-2008.

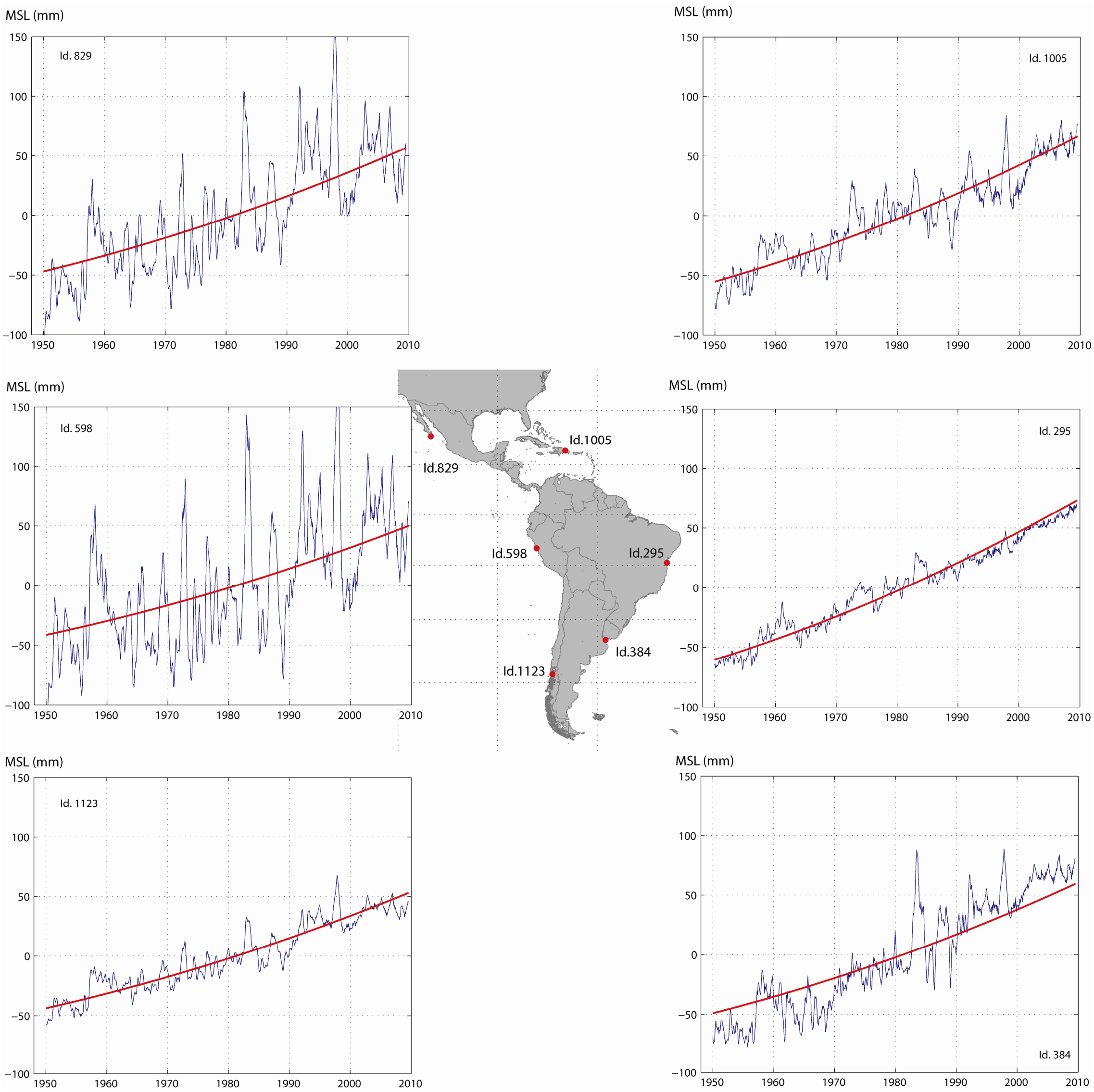

Figure 7. Temporal series for rising sea-levels and the trends obtained (using Trend-EOF) for various representative points in study area.

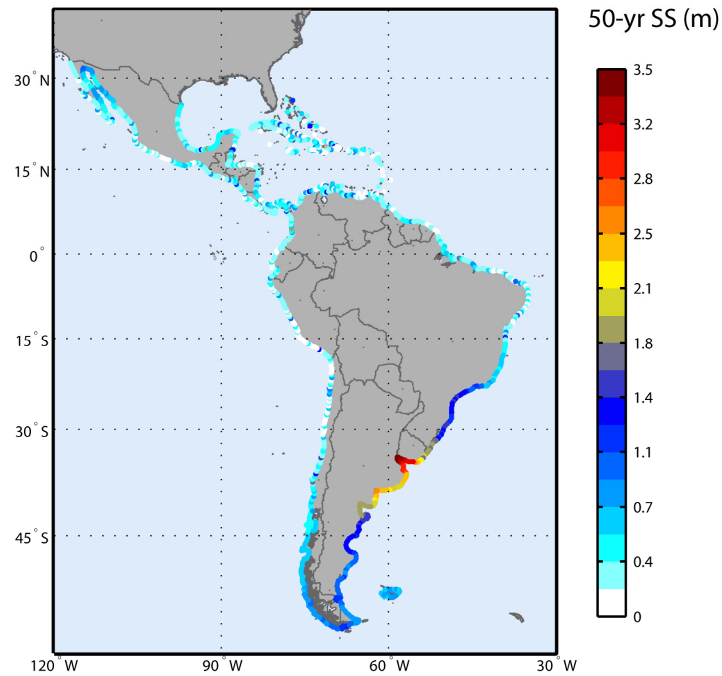

Figure 8. 50-year return period Storm Surge height, obtained by hindcast from 1948 to 2008.

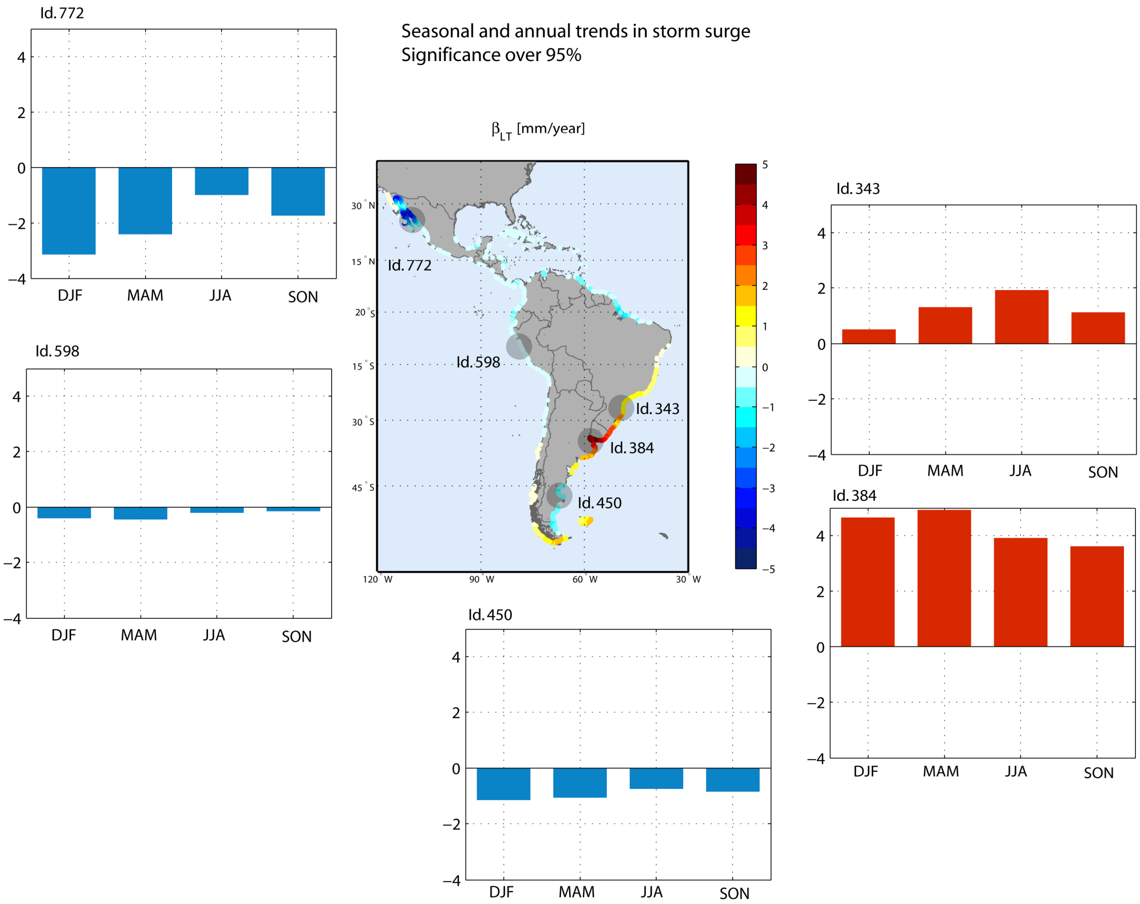

Figure 9. Long-term trends in Storm Surge extremes excluding hurricanes and corresponding seasonal trends at some representative points (mm/yr). The map in the centre shows the annual trend while the adjacent panels represent the seasonal trends at the representative points marked in the map.

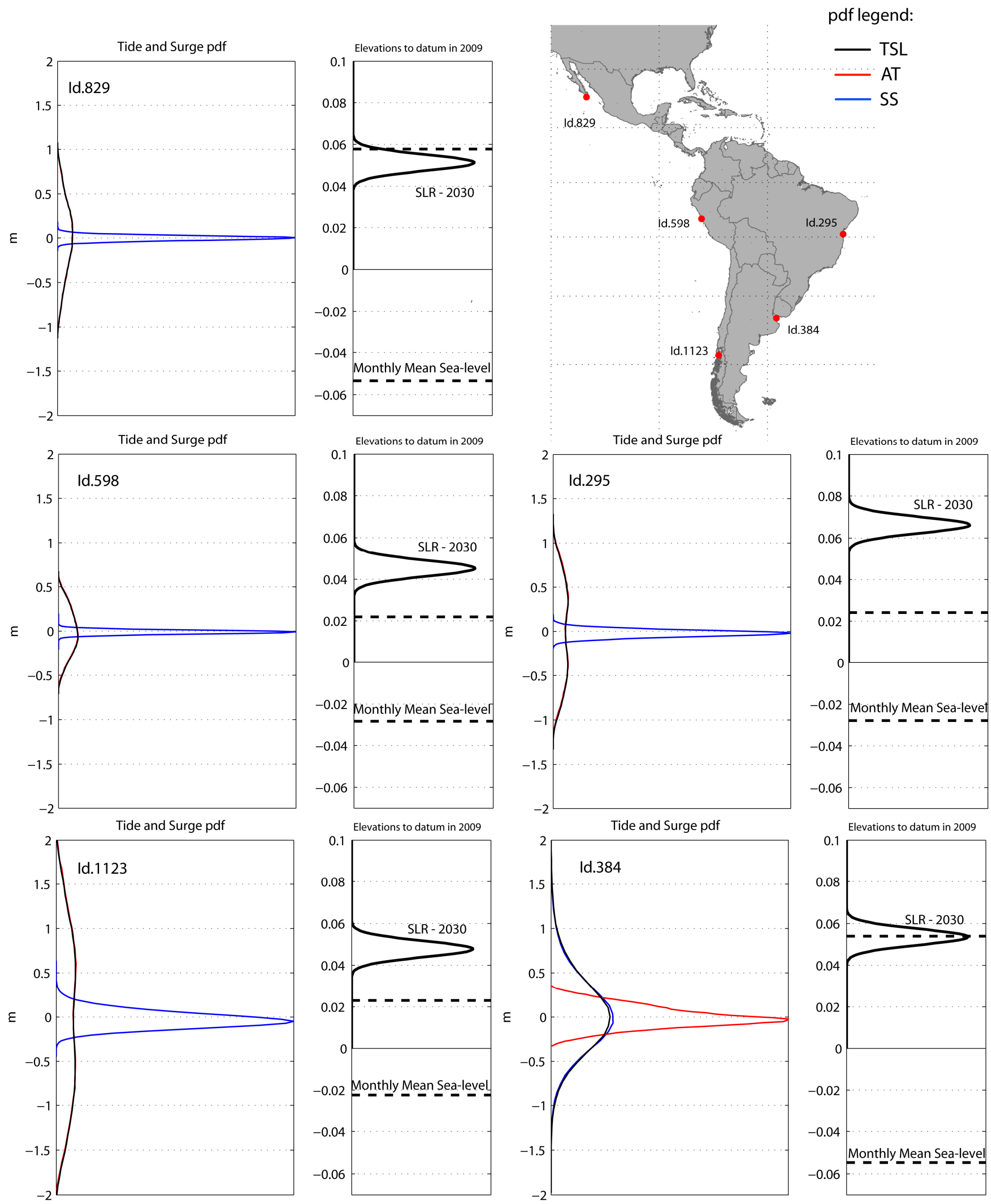

Figure 10. Panels illustrating the relative weight of each sea-level component at various representative points. Panels on the left: probability density functions (pdf) of the Astronomical Tide (red), the Storm Surge (blue) and Total Sea-Level (black). Right panels: Mean Sea-Level seasonality range (broken black line) and probability density function of rising sea-level in 2030 from extrapolation of trends (solid black line). TSL: Total Sea-Level; AT: Astronomical Tide; SS: Storm Surge; SLR: Sea-Level Rise.

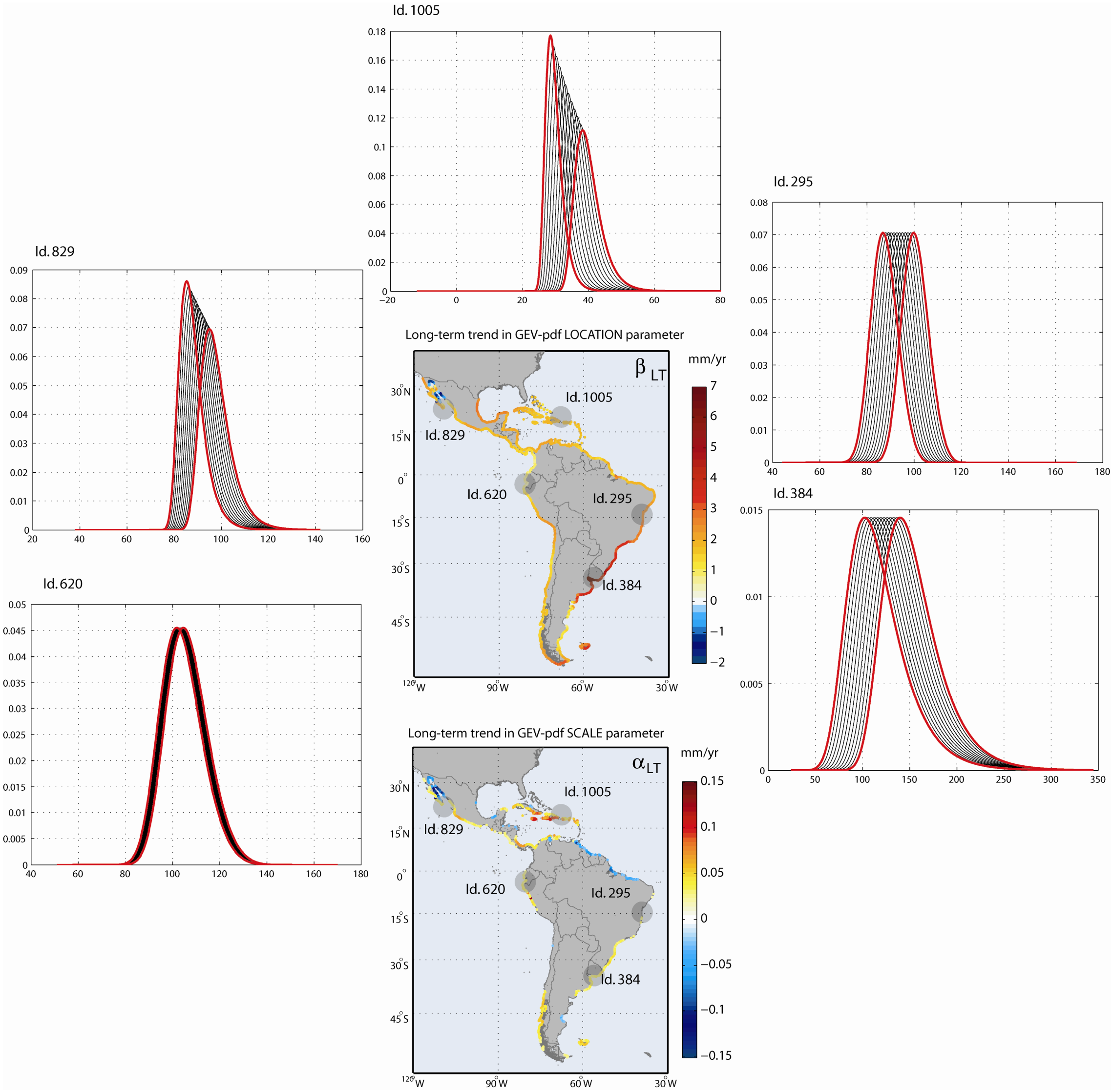

Figure 11. Long-term trend coefficients of the location (upper panel) and scale (lower panel) parameters of the GEV probability density function of extreme levels of the Total Mean Sea-Level and temporal evolution of several probability density functions at certain points of study. Probability density functions are represented at 5 years lapses, the red lines corresponding to the initial (1950) and end (2008) years.

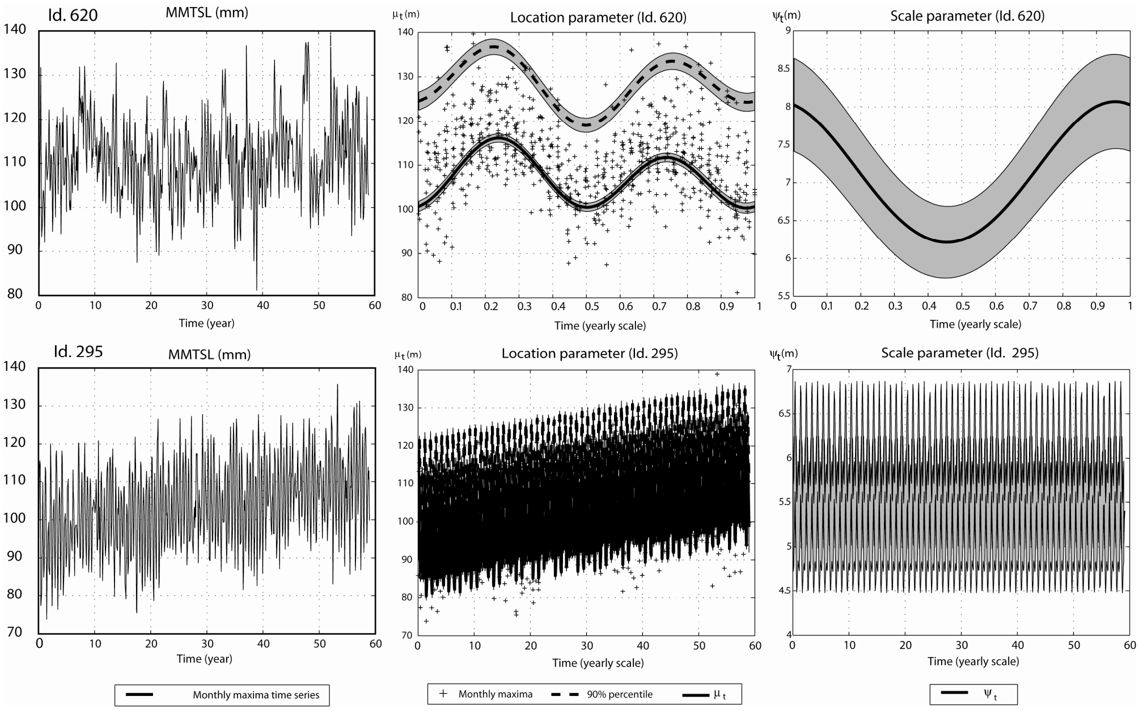

Figure 12. Series of Monthly Maxima of Total Sea-Level (MMTSL; lines in left panels), location (central panels) and scale parameters (right panels) determined for two domain points: 620 (top panels) and 295 (bottom panels). The x-axis represents a temporal scale of years (years from 1950 to 2008 ranging from 1 to 59) when corresponding to time series in which the parameters revealed a significant trend (Id.295) and on an annual scale (representing the months ranging from 0 to 1 year) when the trends were not significant (Id. 620). For the cases of the location and scale parameters (central and right panels), the cruxes represent the monthly maxima data, the dashed line the 90% percentile, the continuous lines the fitted model and the shaded areas the 95% confidence intervals.

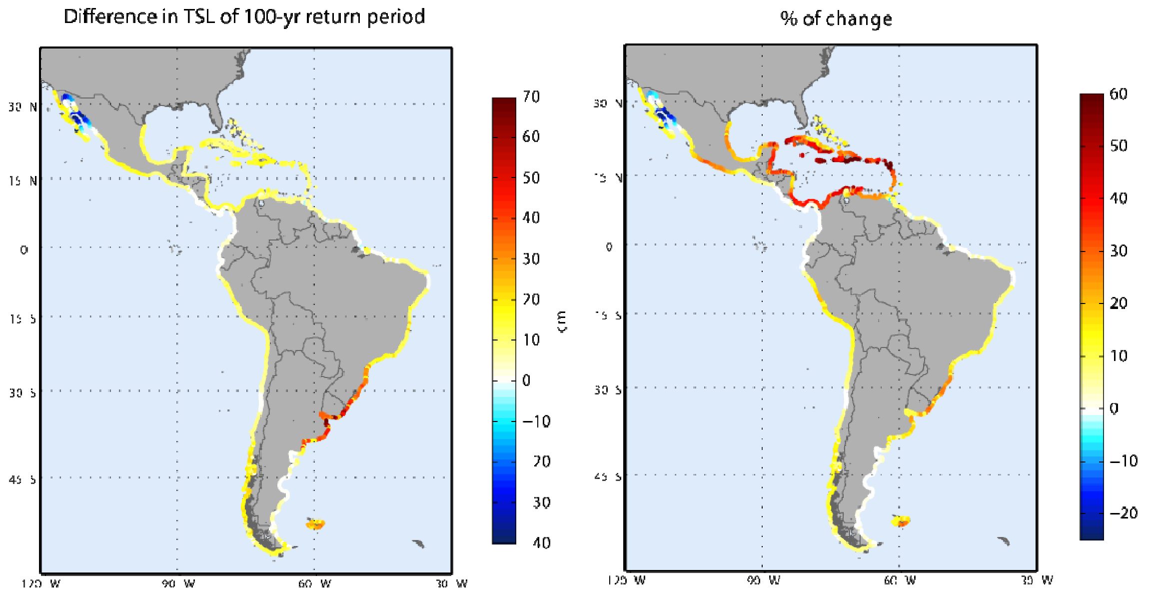

Figure 13. Differences between 100-year return period sea-level values during the first and last decade with available data (left panel). Percentage of change of such difference relative to the value associated with the 100-year return period obtained in the first decade of data (right panel).

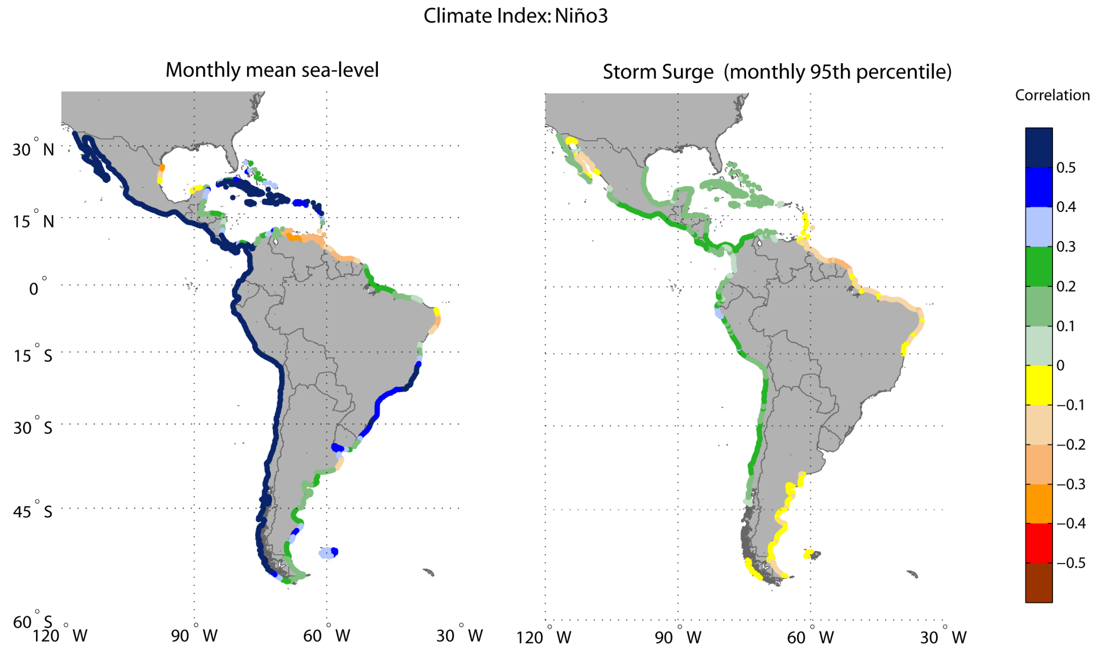

Figure 14. Influence of Niño3 index in the Mean monthly Sea-Level (left panel) and the 95th percentile of Storm Surge (right panel) in terms of the Pearson's correlation coefficient.

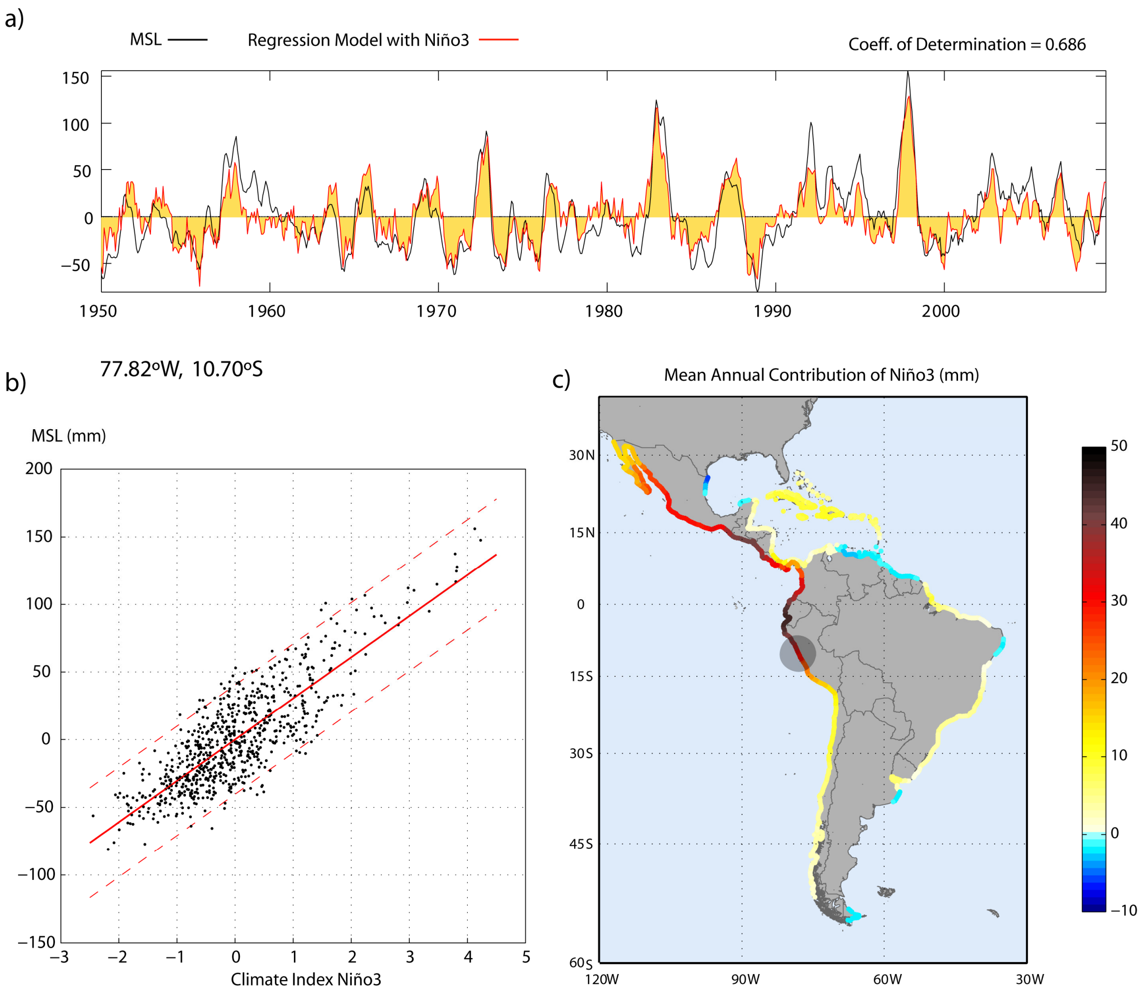

Figure 15. (a) Sea-level time series at a point on the Pacific coast (77.82ºW, 10.70ºS) (black line), and time series reconstructed using the linear regression model with the Niño3 index (red line); (b) dispersion graph and regression line between the Niño3 index and Mean Sea-Level (mm), 95% confidence bounds for a new observation are represented by dashed red lines; (c) average annual contribution to Mean Sea-Level (mm) per unit of Niño3 index (standardized index).